



Experimental characterization and fatigue behavior of thermally and mechanically treated 316L stainless steel MIG-welded joints

Hichem Guizani^{1,2} · Brahim Tlili² · Moez Chafra³

Received: 3 April 2020 / Accepted: 15 September 2020 / Published online: 2 October 2020
© International Institute of Welding 2020

Abstract

The improvement and optimization of post-weld treatments in the case of austenitic 316L stainless steels are, to a large extent, a condition of the service life of the associated structures. In this regard, mechanical brushing and heat treatment are post-weld techniques dedicated to the assembly of mechanically welded structures applicable in the aeronautics, food, and transport sectors. In this study, two techniques are applied to welded joints: mechanical brushing and heat treatment at high temperature. The base material is austenitic stainless steel with molybdenum (AISI316L) in sheet of 5-mm thick. The adopted welding process is Arc Welding under Metal Inert Gas (MIG). Monotonic Tensile test, micro-hardness measurement, low cycle fatigue, micro-hardness measurement, and MES (scanning electron microscopy) observation were conducted in order to qualify the welded, brushed, and heat-treated weldment. Compared with the welded and brushed samples, the treatment with heat annealing specimen maintains the longest lifetime and the lowest consolidation stress $\pm 0.4\%$ imposed strain rate and $10^{-3}/s$ as displacement speed. The annealing heat treatment has a softening effect on the welded structure during the test of the cycle fatigue; this is consistent with the micro-hardness levels measured in the weldment.

Keywords Cyclic behavior · Stainless steel · Mechanical brushing · Annealing · Micro-structure

1 Introduction

Several studies have dealt with various technics for post-treatment of welded joints. They have revealed that such techniques improve the fatigue strength of the welded steel structures. These techniques can be classified in weld geometry improvement methods and residual stress methods [1, 2]. Mechanical and thermal post-welding treatment techniques are applied in order to overcome the effects related to fatigue failure of welded joints [3]. The post-treatment techniques

such as re-melting, shoot peening, grinding, ultrasonic peening, and special welding techniques allow a smooth transition between the different zones of the weldment, reducing the stress concentration. Mainly, this results in an extended crack initiation phase in the fatigue life. As reported by Kim et al. [3], these methods are usually applied to improve the fatigue strength of steel structures after welding and to extend the fatigue life of the treated specimen [4], in the context of mechanical brushing.

Weiss et al. [5] and Schwind et al. [6] suggested respectively element addition technique nitridation, carburization etc.) and welding procedure controlling in order to improve the strength of the weld. The post-weld heat treatment is also considered as a possible remediation. Generally, austenitic stainless steel could not be strengthened by the heat treatment. Thus, the heat treatment is only used in the case where a severe corrosion takes place to reduce the residual stress and improve the corrosion resistance. However, it has been reported that the creep-fatigue resistance cannot be enhanced by heat treatment in 316L austenitic stainless steel [7].

The austenitic stainless steel weldment is susceptible to sensitization after post-weld heat treatment at around 873 K for the relief of the residual stress [8]. Moreover, Liu et al. [9]

Recommended for publication by Commission XIII - Fatigue of Welded Components and Structures

✉ Hichem Guizani
guizanihichem@yahoo.fr

¹ Laboratory of Applied Mechanics and Engineering (LR-MAI): National School of Engineers of Tunis, University of Tunis El Manar, Tunis, Tunisia

² ISET, University Campus of Boulifa, Kef, Tunisia

³ Applied Mechanics and Systems Research Laboratory, Tunisia Polytechnic School, University of Carthage, Tunis, Tunisia

reported that after a long-time exposure to high temperature, δ -ferrite is easy to transform into carbides and some other kinds of brittle inter-metallic phase, which adversely affect the toughness. Therefore, special attention should be paid to the selection of heat treatment conditions to avoid the harmful side effects [9].

In the present paper, two treatments are applied to an austenitic stainless steel SS316L grade, after being welded by the MIG process. These two techniques consist of a heat treatment of hyper quenching and a mechanical brushing by fiber disc brush. The two treatments are carried out separately on joints welded in two passes. The objective of our study is to assess the effects of two thermal and mechanical treatments, on the behavior in monotonic tensile test and cycle fatigue, on micro-hardness, and on the evolution of the micro-structure in the welding zone (the heat affected zone and the melted zone).

2 Experimental protocol

2.1 Preparation and welding

A stainless steel 316L sheet with a thickness of 5 mm is welded by Metal Inert Gas/Arc Welding Gas Metal (MIG/GMAW) process in two passes (Fig. 1). The used shielding gas is 90% of Argon and 10% of CO_2 , and is suitable for the welding standards of stainless steels. The reason for going with 10% CO_2 is that this gas contributes to the stabilization of the regime of the electric arc in MIG/MAG welding [10, 11]. The chemical composition (wt%) and the mechanical properties of the base material, 316L austenitic stainless steel, are listed in Table 1 (the gage length: 12.4 mm).

The preparation of the edges as well as the geometry of the specimens is shown in Fig. 1.

The operating conditions of the welding are summarized in Table 2.

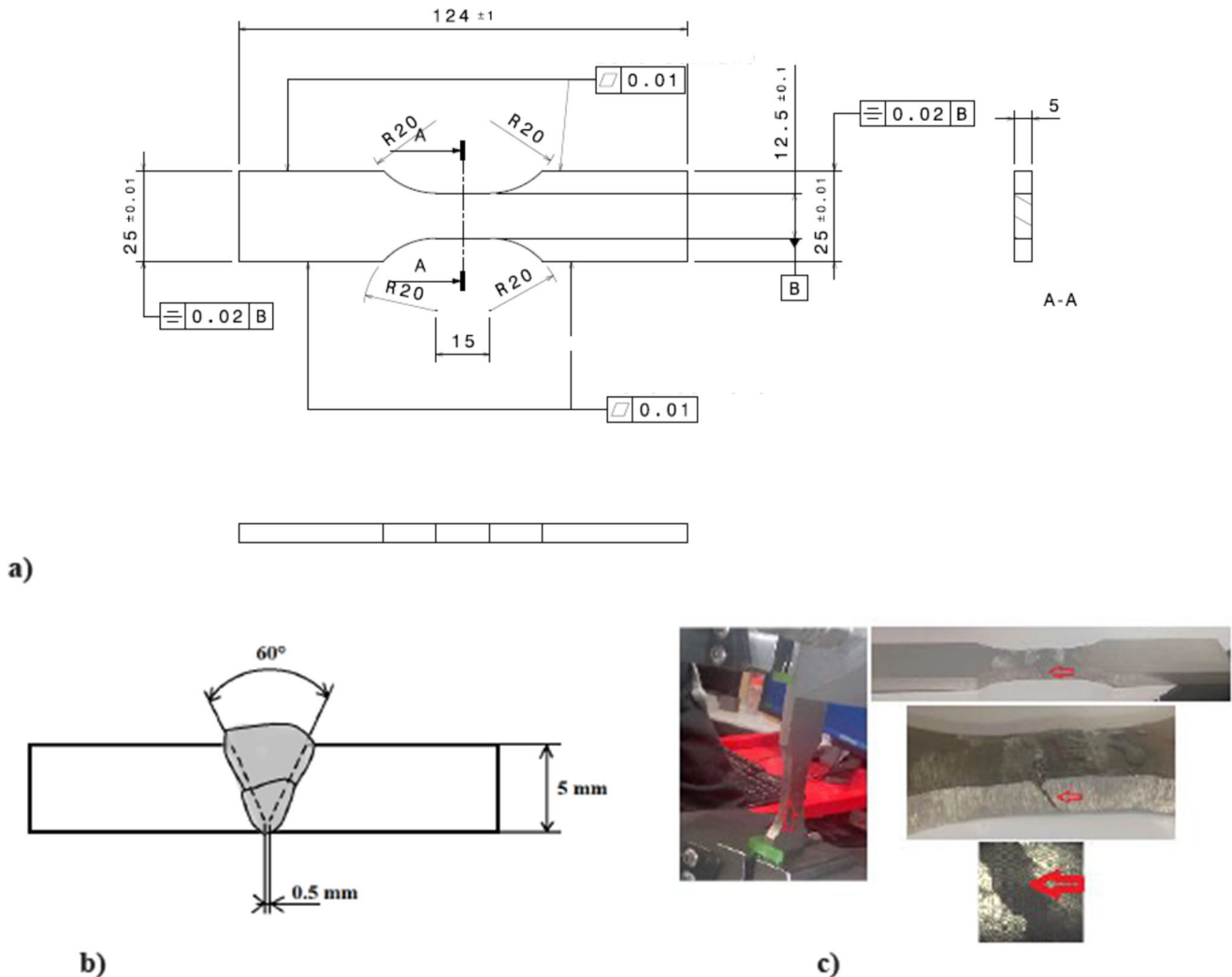


Fig. 1 (a) Fatigue specimen dimensions. (b) Welded sheet metal. (c) Tested and damaged specimen

Table 1 Chemical composition and mechanical properties of the base material

AISI316L	Fe	Cr	Ni	Mo	Mn	Si	Co	Cu	C (%)
	Balance	18.63	9.05	2.42	2.1	0.95	0.21	0.21	0.03
	Yield stress (MPa)		Tensile strength (MPa)		Elongation (%)		Young modulus (GPa)		Poisson ratio
	195		515		28		193		0.29

2.2 Filler metal

The filler metal consists of a solid wire (diameter equal to 0.8 and 1 mm) made of stainless steel AISI308L supplied by the manufacturer FIREP. The mechanical properties and chemical composition (wt%) are shown in Table 3 (the gage length: 12.4 mm).

2.3 Brushed specimen

Samples were brushed under conditions according to our previous work [12] (Table 4).

Table 5 shows the dimensions of the brush used in the brush finishing process of the welded joints.

2.4 Heat-treated specimens

For the annealed specimen, the operating parameters of the thermal treatment are conducted in accordance with Table 6.

During the heat treatment, the samples are maintained at a furnace temperature of $TH = 1100\text{ }^{\circ}\text{C}$ for $tH = 120\text{ s}$ and then quenched with circulating water at $20\text{ }^{\circ}\text{C}$. The levels of the two parameters tH and TH are based on preliminary works and bibliographic reviews [13–17]. In order to avoid residual deformation, oxidation, and excessive aging, these parameters are chosen according to the thickness of the specimens [18]. We use a high furnace temperature in order to overcome or clear some welding operation effects, like the formation of residual ferrite phase and the residual stress of thermal origin.

3 Results and discussion

3.1 Micro-hardness evolution

In the case of the annealed specimen (WAS), the micro-hardness profile is more regular than that of the welded sample (WS: which is the reference sample) that means

absence of ridges and wells of micro-hardness distribution. In the case of the welded and brushed specimen (WBS), there is a total absence of the hardness wells (Fig. 2). The minimum value in the heat affected zone (HAZ) is reached for the reference samples WS: $HV0.2 = 150.1$, and the maximum value is reached for the brushed samples: $HV0.2 = 225$. In the melted zone (MZ), the micro-hardness decreases with 5% by treatment at high temperature and increases with 10% by mechanical brushing of the welded joints.

Mechanical brushing remarkably increases the micro-hardness at the surface of the samples in all areas of the weld. However, heat treatment softens the weld but eliminates micro-hardness peaks between the various areas of the weld. In this case, the profile of the micro-hardness is more homogeneous. At the same treatment temperature ($1100\text{ }^{\circ}\text{C}$), the found results are the same as those obtained by Kamariah et al. [19] and Sistiaga et al. [20] using the same material of our study.

This softening is the result of the implementation of forced micro-structural magnification by heat treatment [19]. It is worth noting that the ferrite phase δ is harder than the austenite phase. Consequently, the reduction of the δ content by transformation following the heat treatment leads to the lowering of the hardness in the 316L welded joints. This is supported by the studies of Yadollahi et al. [21] and others [22, 23].

3.2 Cyclic behavior of welded joints

The study of the cyclic behavior of MIG-welded 316L austenitic stainless steel is carried out on the basis of tensile-compression tests conducted at different levels of imposed total deformation amplitude, using an extensometer with a gauge length equal to 12.5 mm and an opening between extensometer's spouts of 10 mm. These tests are performed until the stress-strain buckles stabilize. The used test pieces are as follows: welded WS, welded and brushed WBS, and finally, welded and annealed one WAS.

Table 2 MIG welding parameters

Parameters	U (V)	I (A)	V_s (mm/s)	En (kJ/mm)	Q_v (l/min)
First pass/second pass	24–26	120–150	3,3–4,1	0,8–0,9	18

Table 3 Mechanical properties and chemical composition (wt%) of the filler material

AISI308L	Fe	Cr	Ni	Mo	Mn	Si	C (%)
	Balance	18.5	12.2	2	2	1	0.03
	Yield stress at 0.2% (MPa)		Tensile strength (MPa)		Elongation (%)		Young modulus (GPa)
	195		515		28		194

3.2.1 Stress-strain hardening

Welded reference joints WS The preliminary tests are carried out at an imposed total deformation amplitude of $\pm 0.4\%$ with a loading ratio $R = -1$ and a frequency $f = 0.5$ Hz. In Fig. 3, an example of the curves of cyclic hardening until rupture is presented, obtained on the welded joint during our study.

For the value of imposed $\Delta\epsilon/2 = \pm 0.4\%$ (Fig. 3 (a)), the loops are symmetrical and regular reaching stress limits of ± 280 MPa of zero mean value. For the last 100 cycles (Fig. 3 (b)), the loops are clearly open showing a high plasticity at this level of deformation. This level of stress can be explained by the presence of precipitates in the filler material preventing the movement of dislocations [24]. Other studies confirm these results by the fact that austenitic stainless steels tend to form, under a cyclic loading, walls, persistent slip bands, and cells which are obstacles to the dislocation movements [25].

Before breaking and for the last 100 cycles, a noticeable drop in stress amplitude is observed as well as a marked tightening of the openings of the loops due to damage at the separating zone of the base material and that of the filler metal (Fig. 1 (c)).

Comparison of the cyclic behavior of the three samples The same loading conditions of section are used to carry out the same tests on the three samples: WS, WBS, and WAS. Figure 4 shows the stabilized loops corresponding to the cyclic behavior of the three grades of the test pieces.

The imposed behavior at deformation of $\pm 0.4\%$ on the brushed and annealed variants shows considerable variability compared with the reference one in terms of stress amplitude and plastic strain.

There is an asymmetry of the loop compared with the loop of the WBS brushed weld and that of the WS reference. These latter loops are more oriented towards compression with stress

amplitudes $\Delta\sigma$ of 290 MPa and 470 MPa, respectively. On the other hand, the loop of the hyper-tempered sample WAS is perfectly symmetrical with $\Delta\sigma = 560$ MPa. The asymmetry of the loop disappears after heat treatment at 1100 °C of the welded joints.

The WS and WBS samples have a pronounced resemblance in compression and a slight difference in the tensile zone of the loop. This small difference on both sides can be explained by the contribution of mechanical brush finishing in terms of surface hardening and its limitation to the surface. The slight dissimilarity of the cyclic behavior indicates that mechanical brushing has an effect on the behavior of the welded joints of steel grade 316L.

Comparison of monotonic and cyclic behaviors In Fig. 5, both the cyclic and monotonic behaviors of the different samples are exposed.

The movement speed of the jaws of the machine for both types of loading is of the order of 10^{-3} s^{-1} . In all the three cases, the cyclic behavior reflects the same aspect of the monotonic loading in traction. The brushed sample WBS is the most compliant for both types of loading. Early stabilization at the imposed strain $\Delta\epsilon/2 = 0.35\%$ is noted for the untreated material. For the brushed sample, stabilization is around $\Delta\epsilon/2 = 0.55\%$ and for the hyper-tempered sample, it is of the order of $\Delta\epsilon/2 = 0.45\%$.

Ductility is well marked for the heat treatment inducing the widest hardening field among the three cases. The stress level reached in annealed case is the lowest. The latter also has the largest elastic domain among the three specimens. The stress levels are high in the hardening zone of the brushed material. The hardness levels in the surface layers, revealed in Fig. 2, may explain the premature plasticization of all these samples. It should be noted that

Table 4 Brushing parameters [12]

Parameters	Va (mm/min)	Nb (rpm)	En (%)	Np (–)
Levels	126	920	4	9

Where Va is the sample feed rate, Nb is speed rotation of brush, En is brush filament penetration rate [12], and Np is the number of brushing passes

Table 5 Characteristics of the brush

Brush diameter	$D_b = 250$ mm
Diameter of the filaments	$D_f = 0.1$ mm
Length of the filaments	$L_f = 80$ mm
Filaments material	Stainless steel
Width of the brush	$l_b = 30$ mm

Table 6 Heat-treatment parameters

Parameters	Maintaining time tH (s)	Holding temperature TH (°C)
Value	120	1100

brushing induces a hardness gradient between the surface and the core of the material.

The hardening work is accompanied by a significant increase in the case of the heat treatment leading to a considerable mechanical resistance in comparison with the reference and brushed samples; this is largely explained by the relaxation of the residual stresses resulting from the welding process and the almost complete transformation of the ferrite into austenite [26]. On the other hand, a loss of ductility appears obvious for a heat treatment of this type. The ductile zone is the most extended for the reference case. Ward et al. [26] concluded that the tensile ductility for austenitic stainless steel of the 316 family depends on and can even be controlled by the morphology, distribution, and stability of the δ phase. This result is proved by several literatures. In the studies carried out in [27–31], the authors concluded that the rupture often begins near the ferrite phase or at the edges delimiting the ferrite-austenite phases. At the end of the monotonic traction test, the rupture of the specimens takes place in the same location which is the bonding interface between the base material and the melted zone.

The relatively low hardness of the quenched material gives rise to high ductility compared with the other two tested samples. Although the brushed sample shows the highest hardness, its ductility range is comparable with that of the reference (i.e., non-brushed and welded) sample. For this reason,

the effect of hardening by mechanical brushing of the surface layers is limited for our 5-mm thick samples.

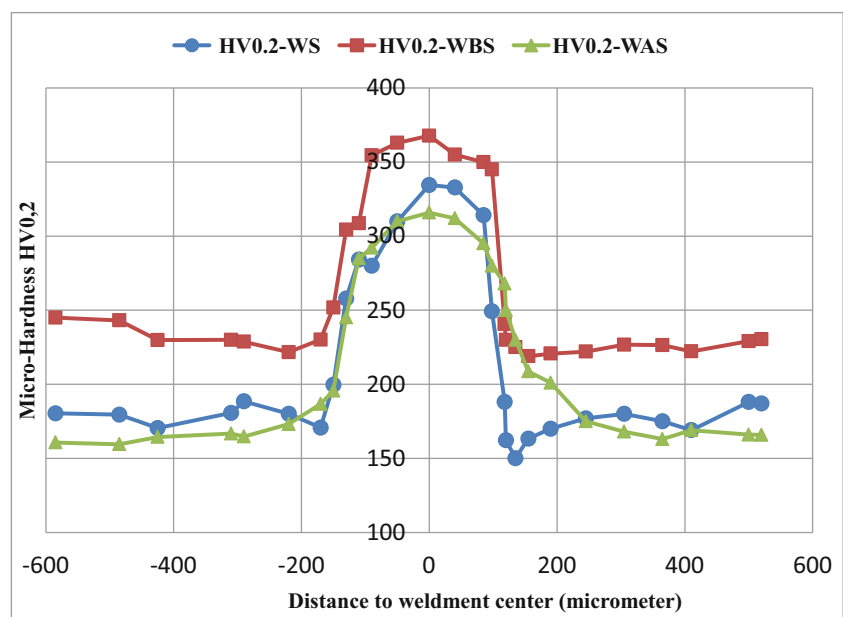
4 Cycle fatigue

4.1 Fatigue life

To obtain the curves of evolution of the stress amplitude $\Delta\sigma/2$ (MPa) as a function of the service-life (N cycles), the tests of the cycle fatigue are carried with an imposed amplitude of strain of $\Delta\varepsilon/2 = 0.4\%$, a frequency of 0.3 Hz, and a strain rate of 10^{-3} s^{-1} . The obtained results are depicted in Fig. 6.

All the samples undergo a pronounced hardening from the first tens of cycles: 50 cycles for the reference sample, 30 cycles for the brushed sample, and 110 cycles for the super-saturated sample. Beyond this plateau, the hardening continues but with a lower slope and remains considerable. Stabilization is noted for the various specimens but at distinct levels of stress and cycle number. The WAS over-tempered sample takes a greater cycle number in this stage whereas the stress level of the WBS and the reference WS only stabilizes for a shorter cycle number range. At this stage of stabilization, the reached stress levels are high in the case of WS and WBS, and are significantly higher compared with the case of WAS. Heavy brushing affects the stress levels in general and especially allows them to reach the peak. The 3 cases are the seat of a subsequent softening until the final rupture. The softening interval taken by the WAS sample is wider than that of the reference WS and the WBS. On the contrary, the

Fig. 2 Profile of micro-hardness in the weld zones of samples WS, WAS, and WBS



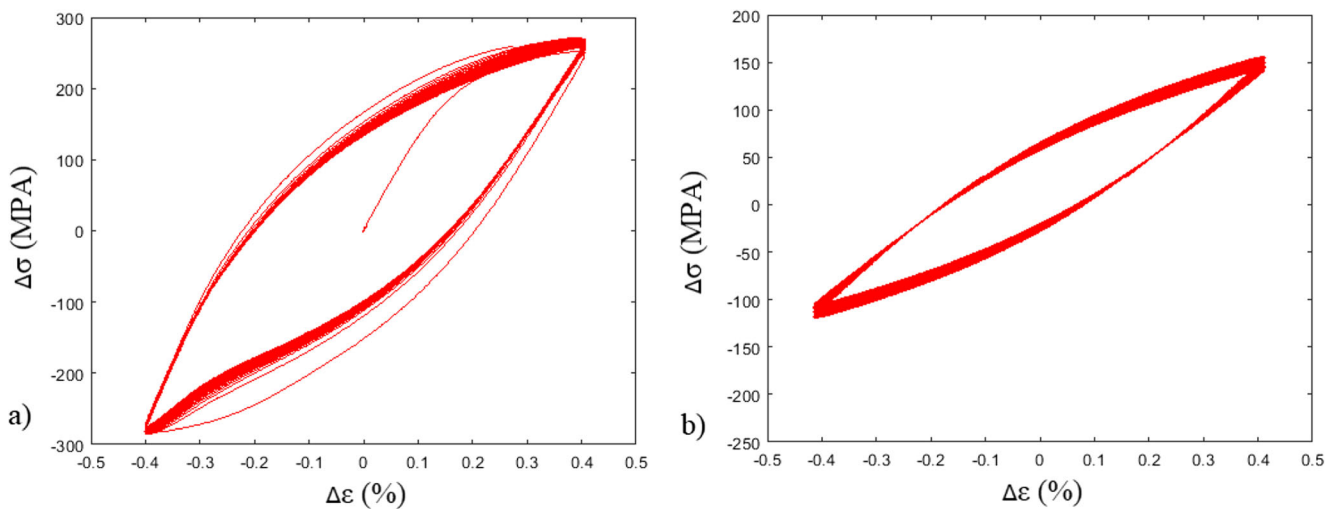


Fig. 3 Cyclic hardening curves of the welded joint: reference sample WS. (a) 100 first cycles. (b) Last 100 cycles before failure

number of cycles at the final rupture is very important for the heat-treated specimen.

For an imposed deformation level of 0.4%, the annealed material has the longest life before break. It offers a longer life than the non-treated (reference) sample.

4.2 Cyclic hardening and softening

During cyclic loading of the specimens, there can be a softening, a hardening, or an alternating phenomenon followed by stabilization.

The level of hardening and cyclic softening of the various samples tested in our study are determined according to Eqs. 1 and 2 (Kchaou et al. [25]):

$$\text{Hardening rate} = \frac{\sigma_{\text{pic}} - \sigma_{\text{first cycle}}}{\sigma_{\text{first cycle}}} * 100 (\%) \quad (1)$$

$$\text{Softening rate} = \frac{\sigma_{\text{pic}} - \sigma_{\text{NR}/2}}{\sigma_{\text{first cycle}}} * 100 (\%) \quad (2)$$

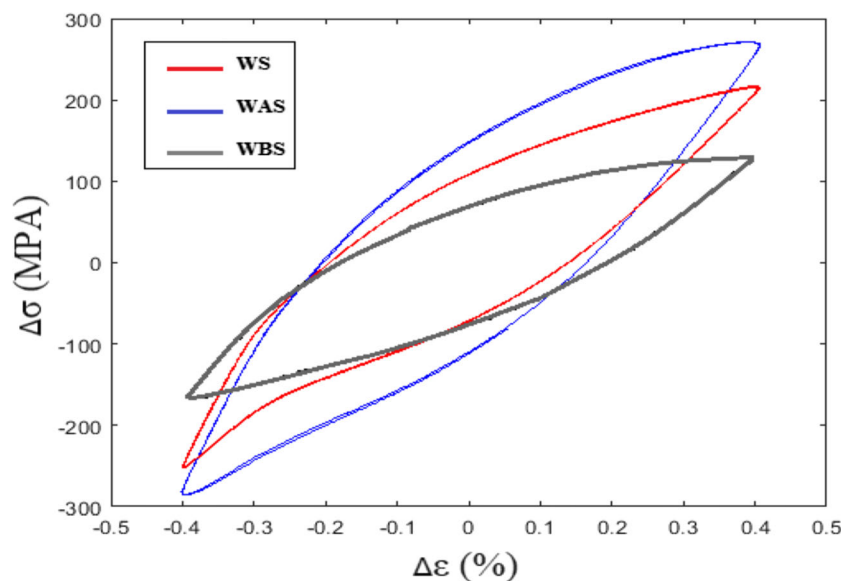


Fig. 4 Stabilized loops of the various samples: $\Delta\epsilon/2 = \pm 0.4\%$, $R = -1$, $f = 0.5$ Hz

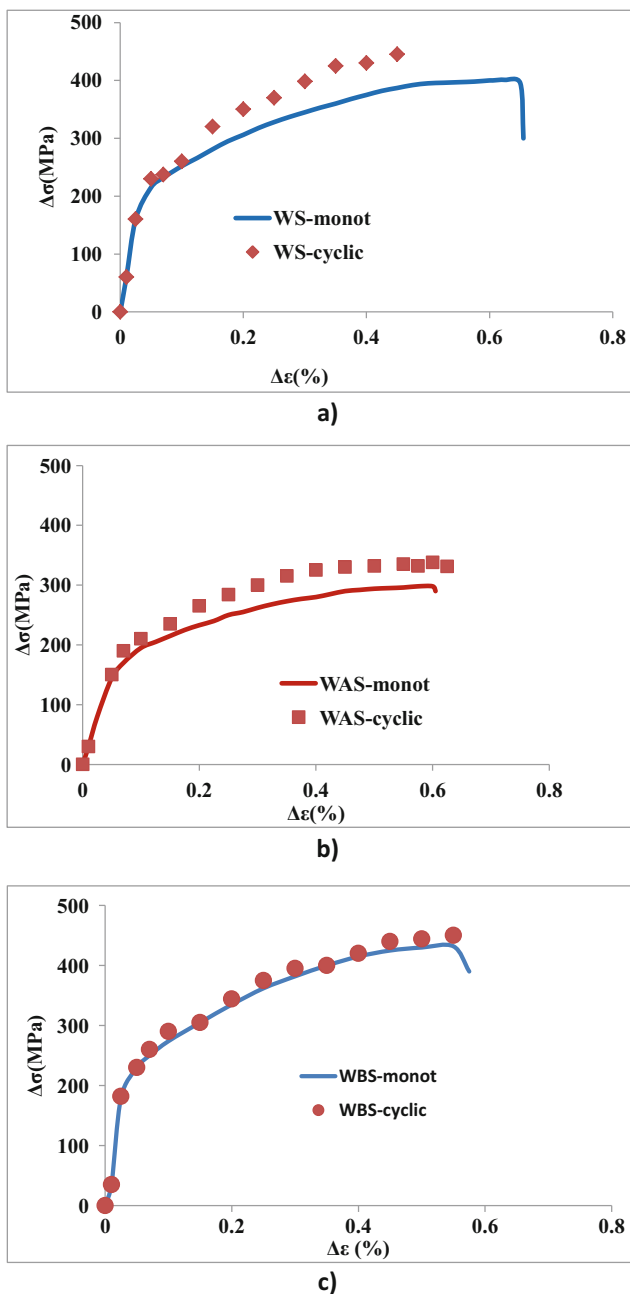


Fig. 5 Comparison of the cyclic and monotonic behaviors of the samples: (a) welded reference, (b) welded and annealed, (c) welded and brushed

All the samples exhibited a hardening then a softening before the final rupture. This is an equivalent behavior of the base material. To highlight these two phenomena, the obtained results are summarized in Table 7.

The appearance of the peak is delayed by 200 cycles after annealing of the welded joint. For the other two cases, this peak appears for comparable numbers of cycles: 30 and 50 cycles, thus indicating an accelerated increase in hardening.

According to Table 7, the heat-treated sample shows minimal hardening and softening compared with the other two specimens. The difference reaches 4% for both phenomena.

4.3 Influence of the loading speed

To profile the influence of the deformation, two levels are operated: $\Delta\epsilon/2 = 0.4\%$ and $\Delta\epsilon/2 = 0.8\%$ while keeping the same speed of displacement at 10^{-3} s^{-1} and a frequency of 0.3 Hz (Fig. 7). Figure 8 shows the curves of the stress variation as a function of the number of cycles for the two strain level and for all the samples.

By increasing the imposed strain from 0.4 to 0.8%, a significant cyclic hardening is noted in all cases. This hardening is much accelerated for the welded and brushed sample. At this stage, high levels of stress are reached.

All the samples undergo softening to failure. However, their range is reduced for high imposed deformations.

For an imposed strain of 0.8%, WS and WBS show similar behavior, whether in terms of cyclic hardening or in the number of cycles at break. This indicates a non-significant effect of brushing at a certain level of loading.

The hyper-tempered specimen keeps the lowest stress level but the longest rupture life compared with the other two cases. The imposed deformation influences the rate of cyclic hardening, the softening interval, and the service life of the various samples. This also illustrates a positive sensitivity of the stresses to the strain rate. This result was found in similar work carried out by De Baglion [32] on austenitic stainless steel 304L under ambient conditions.

For a material of the same family (i.e., SS304), Rao et al. [33] proved that the filler metal of austenitic stainless steel 304 contains a very high density of dislocations. The existence of entangled dislocations as well as fragile (precipitated) particles in the weld is responsible for early hardening during cyclic loading.

Regarding the high softening rate of the welded joint, according to Kchaou et al. [25], it can be explained by the high density of dislocations which annihilate and rearrange into a cellular structure during cyclic loading.

5 SEM analysis

To highlight the mechanisms of damage and the failure of the samples by cycle fatigue, observations are made by scanning electron microscope (SEM) on the failure facies of the tested samples.

5.1 Reference sample: WS

For the most WS samples, the rupture takes place in heat-affected zone and the melted zone as indicated by the initiation of cracks (Fig. 8 (a)). This sample shows a rupture following an internal cracking from the melted zone to the base material. The structure is characterized by the existence of solid particles as well as inclusions

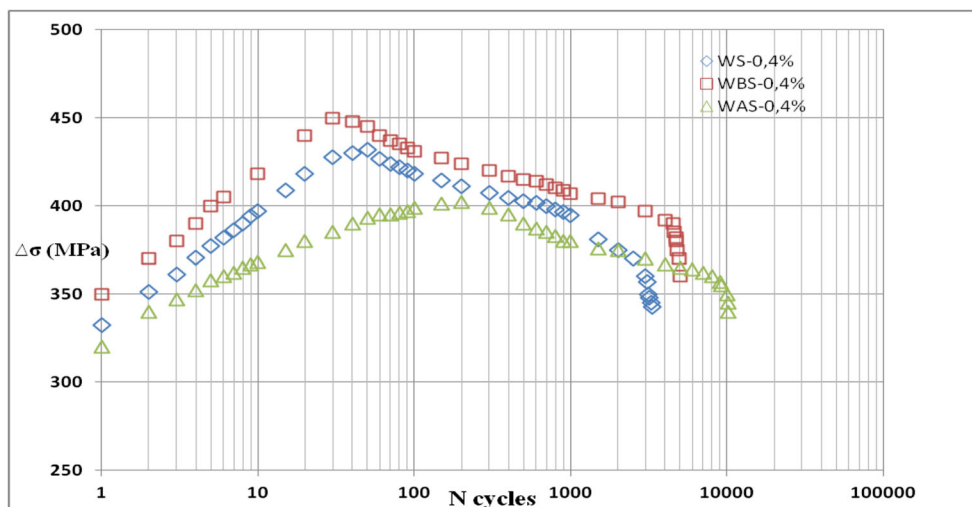


Fig. 6 Evolution of the cyclic stress amplitude for the different samples

acting as obstacles to micro-cracks (Fig. 8 (a, b, and c)). The existence of these obstacles stimulates the coalescence of the cracks and reduces the time life of the specimen. The main propagation zone of the cracks is characterized by a planar ductile striation contrary to the brutal and accelerated rupture zone which is the seat of a three-dimensional cellular structure (Fig. 8 (c)).

The presence of inclusions and solid particles is the main causes of early hardening during cyclic loading and the absence of the stabilization phase (the gamma phase γ).

This is suitable with similar results found by Rao et al. [33], for the welds of austenitic stainless steels 304 cyclically loaded. The authors shown that the filler metal contains a very high density of dislocations of the order of 8.109 cm^{-2} . This high density of dislocations is mainly due to the thermal stresses generated during the welding process. This result is validated by our work for low and high imposed deformation rates ($\pm 0.4\%$ and $\pm 0.8\%$).

In the fracture zone (Fig. 8 (e, f)), the propagation of the micro-cracks is three-dimensional transgranular. The material resulted in the final rupture by tearing and removal of the facies (Fig. 8 (e, d)).

The existence of solid inclusions can be at the origin of:

- Early cyclic hardening and brittle fracture.
- Oxidation zone around the inclusions.

The presence of inclusions and solid or brittle particles in the weld (fracture facies in Fig. 8 (a, b)) has greatly weakened the lifetime in the case of the cycle fatigue as seen before in this paper. This is explained by the initiation of micro-cracks around these inclusions. The favorable rupture zone is the transition zone between the base material and the melted zone. This discontinuity zone is a stress concentration site.

High levels of hardness are observed in the HAZ, which are significantly higher than those taken from the rest of the test sample. This hardening is one of the origins of the brittle fracture during cyclic loading with high imposed deformation.

5.2 Brushed sample

For this case, an early peak of hardening by cyclic loading is obtained in comparison with the other two samples. This relatively premature curing is accompanied by multiple initiations of the fatigue micro-cracks (Fig. 9 (b)). The priming sites are below the hardened layers by mechanical brushing (HLMB) as depicted in Fig. 9 (a). The base material is the favorable site of rupture as well as secondary fatigue cracks.

According to Fig. 9 (a), it is observed that the propagation is obtained in the two directions: in the brushed layers and in the core of the unbrushed material. In the core of the material, SEM observations showed coalescence of fatigue micro-

Table 7 Evolution of the stress amplitudes and the rates of hardening and softening

	$\Delta\epsilon t/2$ (%)	$\sigma_{\text{first cycle}}$ (MPa)	σ_{pic} (MPa)	Cycle pic	$\sigma_{\text{NR}/2}$ (MPa)	Hardening rate (%)	Softening rate (%)
WS	0.4	332.5	431	30	378	29.6	15.9
WBS		350	450	50	400	28.5	14.2
WAS		320	402	200	365	25.6	10.1

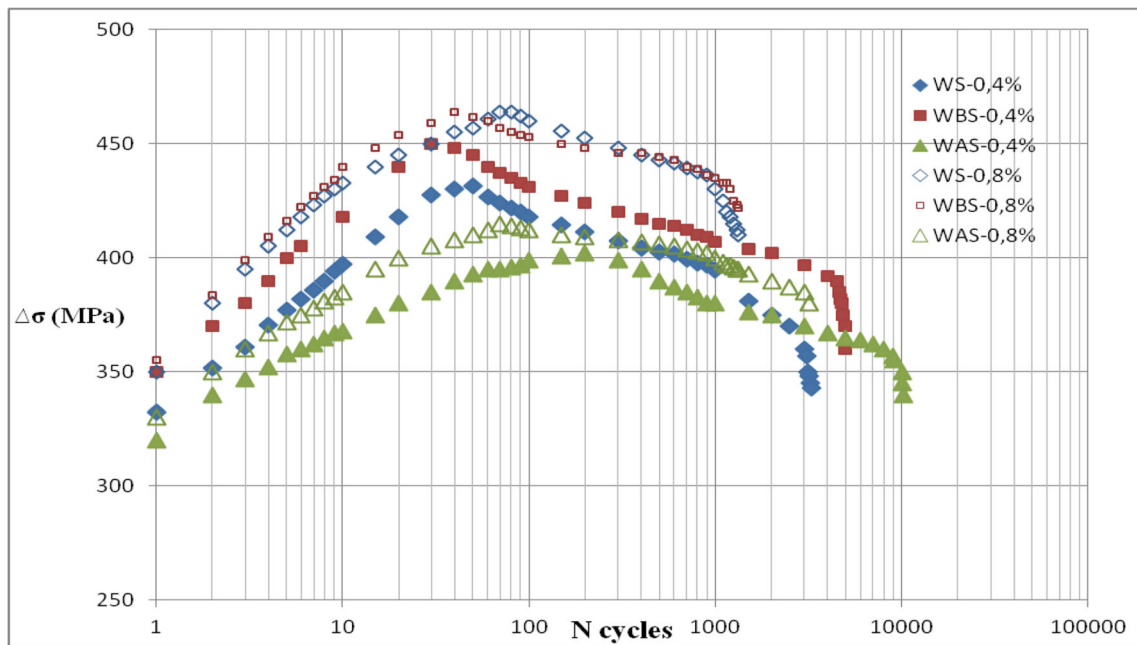


Fig. 7 Influence of the imposed loading speed on the fatigue life of the different test specimens

cracks (Fig. 9 (c, d)). Figure 9 (d) shows an obstacle circumvented by micro-cracks. The saturation in micro-cracks reduces the shearing of the obstacle and gives rise to a cell structure facies (Fig. 9 (e)).

Priming and propagation in the cured area by brushing are more distinguished. The initiation of cracks continues until the final fracture of the sample (Fig. 9

(f, g, h)). The propagation of the fatigue micro-cracks is mainly transgranular (Fig. 9 (h)). The fracture facies is marked by a relief (fragment) following a brittle fracture (Fig. 9 (f)).

The multiple crack initiations under the brushed layers (Fig. 9 (b)) can be explained by the presence of a hardness gradient. The existence of this gradient is proved by micro-

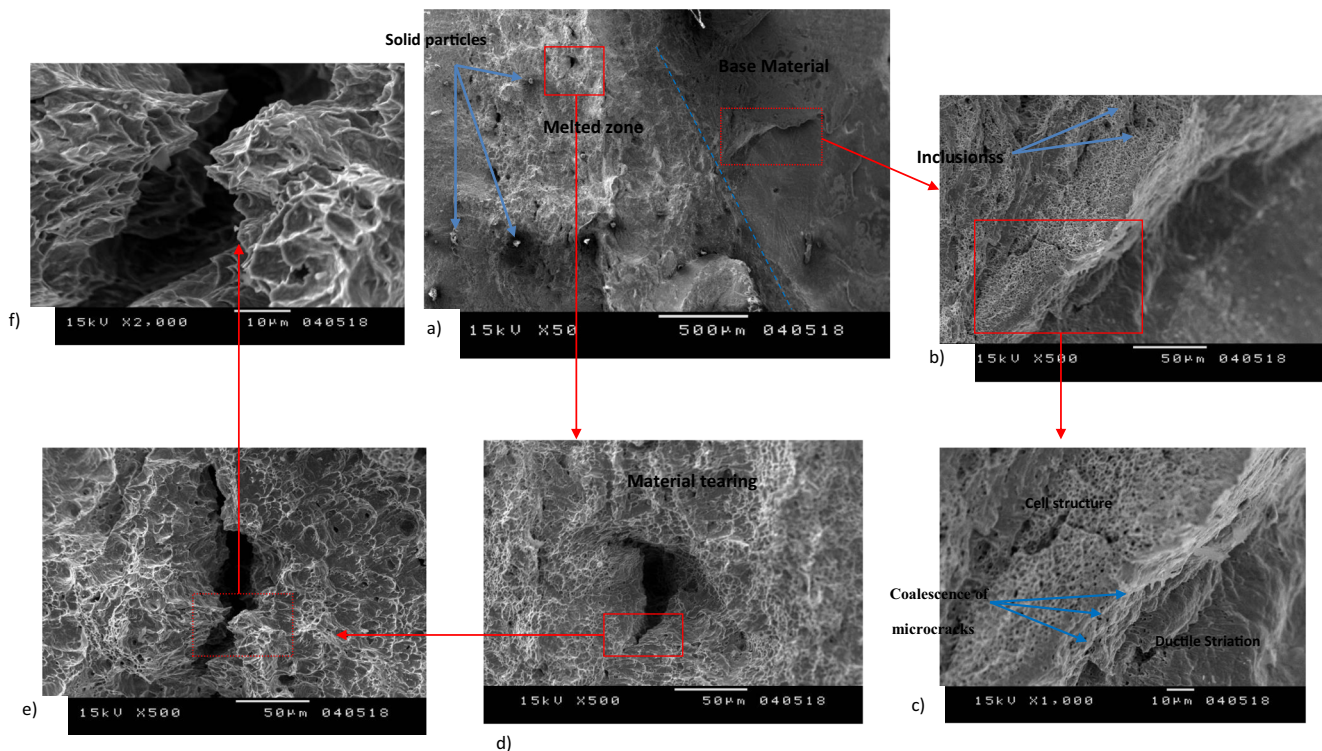


Fig. 8 SEM observation of the fracture facies of the welded sample (WS)

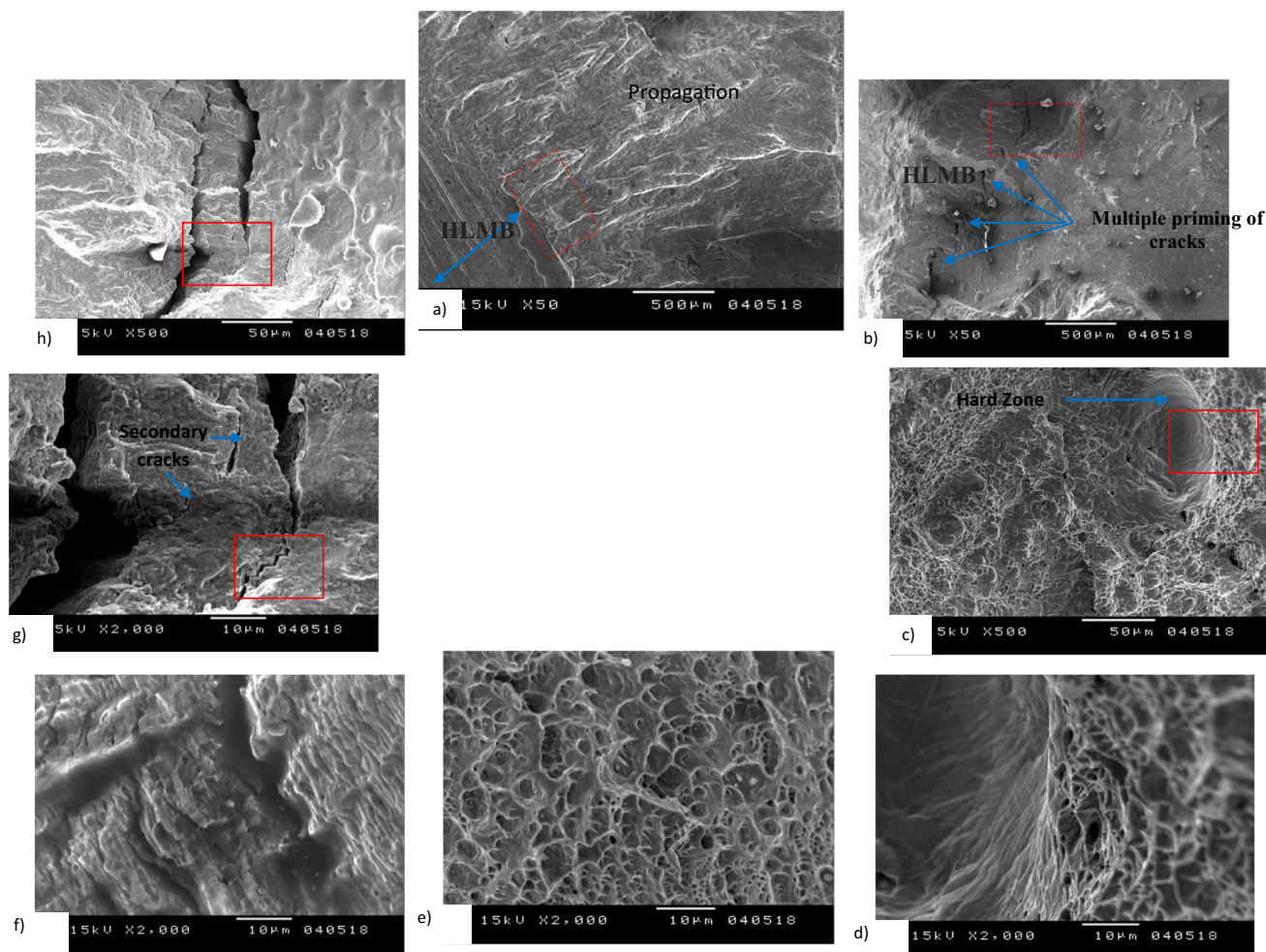


Fig. 9 SEM observation of the fracture facies of the brushed sample (WBS)

hardness measurements. The effect of this level difference in terms of micro-hardness continues until the phase of propagation of fatigue cracks (Fig. 9 (h, g)).

In the case of the brushed samples, the predominant factor influencing the cycle fatigue behavior of the welded joints is the micro-hardness gradient between the surface and the core of the material.

5.3 Heat-treated sample

For the case of the annealed sample, regardless of the loading level ($\pm 0.4\%$ or $\pm 0.8\%$), the saturation peak is the lowest among the three studied cases. The high temperature level and the short holding time could not prevent the formation of oxidation even in very small areas of the welded joint (Fig. 10 (b)). The location of these areas is too close to the surface. This may explain the channel structure after fracture of the sample (Fig. 10 (h)). Beyond these oxidations, priming, propagation, and coalescence take other ways and other forms (Fig. 10 (b, c, j)).

The existence of *precipitates or solid particles including solid inclusions in the weld zone (melted zone and heat affected zone) disturbs too much the dislocation movement. These barriers are either sheared or bypassed* (Fig. 10 (g, f)). A third case noted by our study is the fact that a sufficiently rigid but small obstacle can be ripped leaving a crater void (Fig. 10 (e)). Indeed, the small precipitates are generally coherent with the matrix and are therefore sheared. Large precipitates may be heterogeneous with the matrix, and thus are non-shearable [25]. Hence, barriers of this type favor the multiplication of dislocations [24]. The movement of dislocations blocked by the presence of these precipitates causes the hardening of the material and reduces its ductility and resilience [25]. The growth and coalescence of these micro-cracks lead to the formation of fatigue cracks at the level of several grains which propagate in the ductile bulk material and lead to the fracture of the specimen, as illustrated in Fig. 10 (b). In this figure, existence of the cleavage facets which appeared for a loading of $\pm 0.8\%$ imposed

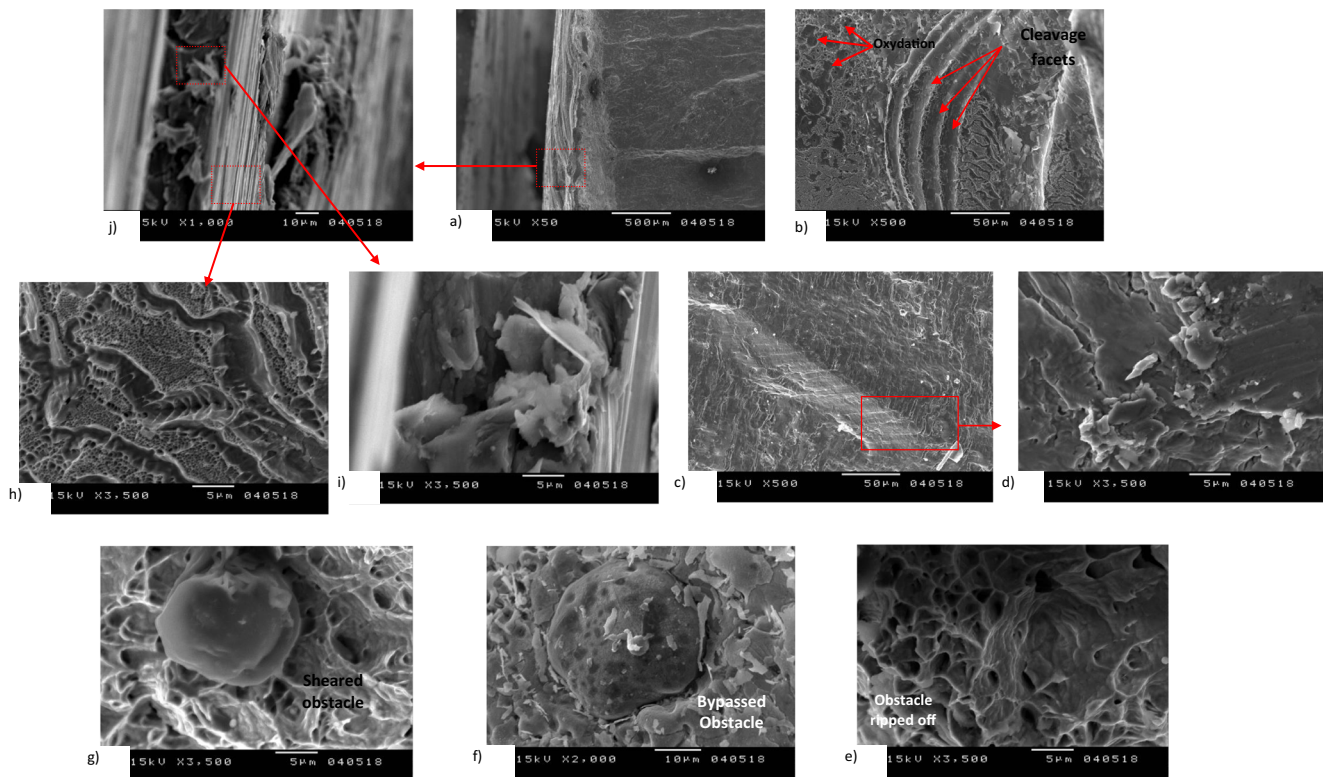


Fig. 10 SEM observation of the fracture faces of the hyper-tempered sample (WAS)

deformation. The probable explanation of the presence of islands of oxidation (even in a small proportion) is the thermal aging.

Figure 10 (c) and (d) indicate the presence of a deviated slip which is the sign of the existence of several paths or dislocation propagation paths. This leads to a three-dimensional damage in the welded structure. These figures indicate propagation-based ductile striation. Thus, it can say that the thermal treatment has a softening effect on the welded structure. This result is confirmed by the study of the micro-hardness.

The softening effect of the annealing treatment is demonstrated by the micro-hardness profile in the welded joint. This treatment has a weakening effect on the solid inclusions, thus allowing them to either tear or shear (Fig. 10 (g, e)) and avoiding the cyclic hardening.

6 Conclusion

The main results of this study are the following:

- The 3 samples show a subsequent softening until final rupture. The softening interval taken by the WAS sample is wider than that of the reference WS and the WBS. On the contrary, the number of

cycles at the final rupture is very important for the heat annealing treatment.

- For an imposed strain level of 0.4%, the brushed material has the longest life just before fracture. It offers a longer life than the unbrushed (reference) sample.
- Compared with WS and WBS, the heat annealing treatment maintains the longest lifetime and the lowest consolidation stress for the various imposed strain rates and the different displacement speeds tested.
- For high loading speeds, the disparities between WS and WBS become smaller. In fact, the cyclic binding curves for the two specimens have the same trends.
- The annealing heat treatment has a softening effect on the welded structure. This result is confirmed by the study of the micro-hardness in the different zones of the welded joint.

In this paper, we investigated the importance and the validity of two types of welded joint finishing treatment which are mechanical brushing and hyper quenching. We were able to relate in a sense between the micro-hardness, the hardening, the micro-structure, and the oligocyclic fatigue life of the reference and treated samples. In this context, the main results of this paper can be a continuation to improve the service life of welded joints of

austenitic stainless steels and overcome the consequences of high heat input welding processes.

References

- Kirkhope KJ, Bell R, Caron L, Basu RI, Ma KT (1999) Weld detail fatigue life improvement techniques. Part 1. *Mar Struct* 12(6):447–474
- Haagensen P, Maddox S (2013) IIW recommendations on methods for improving the fatigue strength of welded joints: IIW-2142-110. Woodhead Publishing
- Kim IT, Kim HS, Dao DK et al Fatigue resistance improvement of welded joints by bristle roll-brush grinding. *Int J Steel Struct* 18(5): 1631–1638
- Ben Fredj N, Sidhom H, Braham C (2006) Effect of the cryogenic wire brushing on the surface integrity and the fatigue life improvement of the AISI 304 stainless steel ground components. In: *Fracture of nano and engineering materials and structures*. Springer, Dordrecht, pp 1303–1304
- Weiss B, Stickler R (1972) *Metallurgical Transformation A* 3:851–866
- Schwind M, Kallqvist J et al (2000) σ -phase precipitation in stabilized austenitic stainless steels. *Acta Mater* 48:2473–2481
- Hert D, Lebrun JP (1996) *Int J Fatigue* 18(1):60
- Yamauchi K (2002) *Metallurgical Material Transformations A* 33A:174
- Liu F, Hwang YH, Nam SW (2006) The effect of post weld heat treatment on the creep-fatigue behavior of gas tungsten arc welded 308L stainless steel. *Mater Sci Eng A* 427(1–2):35–41
- Valensi F (2007) Contribution to the study of phenomena related to anodic and cathodic effects in MIG-MAG welding. *Physics*. University of Orleans, France. fftel-00449180f (<https://tel.archives-ouvertes.fr/tel-00449180/document>)
- Sylwia Zielinska. Physical properties of MIG-MAG plasma. *Process Engineering*. University of Orléans, 2005. France. fftel-00458799f (<https://tel.archives-ouvertes.fr/tel-00458799/document>)
- Guizani H, Nasser MB, Tlili B, Oueslati A, Chafra M (2019) Finishing and quality of mechanically brushed 316L stainless steel welded joints using MIG process: hardness modeling by L9 TAGUCHI design. *Int J Adv Manuf Technol* 105(1–4):1009–1022
- R. N. GUNN. Duplex stainless steels. 2000
- P. LACOMBE, B. BAROUX, G. BERANGER. *Stainless steels*.1990
- Lippold JC D.J. Kotecki, *Welding metallurgy of stainless steel*
- Riad Badji (2008) Influence of high temperature heat treatments on the evolution of texture and microstructure of 2205 duplex stainless steel welds. *Mechanics of materials [physics.class-ph]*. Paris-Nord University - Paris XIII. France. <tel-00806333> (https://tel.archivesouvertes.fr/file/index/docid/806333/filename/PhD_Badji_2008.pdf)
- Kožuh S, GOJI M (2009) Mechanical properties and microstructure of austenitic stainless steel after welding and post-weld heat treatment. *Kovove Materialy* 47:253–262
- Safrany JS *Techniques of the engineer-treaty metallic materials* . M 1(630):1–22
- Kamariah MSIN, Harun WSW, Khalil NZ, Ahmad F, Ismail MH, Sharif S (2017) Effect of heat treatment on mechanical properties and microstructure of selective laser melting 316L stainless steel. In *IOP Conference Series: Materials Science and Engineering* (Vol. 257, No. 1, p. 012021). IOP Publishing
- Montero Sistiaga M, Nardone S, Hautfenne C, Van Humbeeck J (2016) Effect of heat treatment of 316L stainless steel produced by selective laser melting (SLM). In: *Proceedings of the 27th Annual International Solid Freeform Fabrication Symposium-An Additive Manufacturing Conference*, pp 558–565
- Yadollahi A, Shamsaei N, Thompson SM, Seely DW (2015) Effects of process time interval and heat treatment on the mechanical and microstructural properties of direct laser deposited 316L stainless steel. *Mater Sci Eng A* 644:171–183
- Imandoust A, Zarei-Hanzaki A, Heshmati-Manesh S, Moemeni S, Changizian P (2014) Effects of ferrite volume fraction on the tensile deformation characteristics of dual phase twinning induced plasticity steel. *Mater Des* 53:99–105
- Kocijan A, Merl DK, Jenko M (2011) The corrosion behaviour of austenitic and duplex stainless steels in artificial saliva with the addition of fluoride. *Corros Sci* 53(2):776–783
- Friedel J *Dislocations* pergamon, New York, p 274
- Kchaou Y (2015) A comparative study of the mechanical properties of superaustenitic and duplex welded joints in pressure vessels. Dhd, ISAE-ENSMA, Poitiers, France
- Ward AL Thermal and irradiation effects on the tensile and creep-rupture properties of weld-deposited type 316 stainless steel. *Nuclear Technol* 24(2):201–215
- Goodwin GM, Cole NC, Slaughter GM Study of ferrite morphology in austenitic stainless steel weldments. *Welding Res Suppl* (United States)
- Gugelev BM Mechanism of the deformation and fracture of austenitic-ferritic weld metal. *Automat Weld* 22(7):20–23
- Ivanov KM, Petrov GL The thermal embrittlement of chromium-nickel austenitic-ferritic weld metals when aged at temperatures below 500°C. *Welding Research Abroad*:79–85
- Yarkovoi V, Muromtsev B, Komissarov V Long time strengths of parent metal and welded joints in Kh18N9 and Kh16N9M2 steels. *Automat Weld* 22(6):40–43
- Heuschkel J Time-temperature dependence of austenitic stainless steel welded joint components. *Welding J* 35:12
- De Baglion L (2011) Low cycle fatigue behaviour and damage of a type 304L austenitic stainless steel, as a function of environment (vacuum, air, primary water PWR) at 300 degrees Celsius. Dhd, ISAE-ENSMA, ISAE-ENSMA, Poitiers, France
- Prasad R, Rama R (1995) Effect of welding parameters and gas composition on ferrite content of austenitic weld and clad metals. *Prakt Metallogr* 32(6):312–324

Publisher's note Springer Nature remains neutral with regard to jurisdictional claims in published maps and institutional affiliations.